Beryllium and Magnesium Metal Clusters: New Globally Stable Structures and G_0W_0 Calculations

Sunila Bakhsh, Xiaohui Liu, Yanyong Wang, Lixin He, and Xinguo Ren*

Read Online

ACCESS | Metrics & More | Article Recommendations | Supporting Information

ABSTRACT: We study the structural and electronic properties of beryllium (Be) and magnesium (Mg) clusters for sizes 2−20 using a two-step approach. In the first step, a global search of the stable and low-lying metastable isomer structures is carried out on the basis of first-principles potential energy surfaces at the level of the generalized gradient approximation (GGA) of density functional theory (DFT). In the second step, vertical ionization potentials (VIPs) and energy gaps between the highest occupied molecular orbital (HOMO) and lowest unoccupied molecular orbital (LUMO) are determined using the G_0W_0 methods for up to the fourth-lowest-energy isomers. Novel globally lowest-energy isomer structures are identified for Be_{14}, Mg_{14}, and Mg_{16} clusters. The van der Waals interactions are found to have a stronger influence on Mg clusters than on Be clusters. A second-difference analysis for both the binding energies and HOMO−LUMO gaps reveals a close relationship between the structural stability and chemical hardness for both types of clusters.
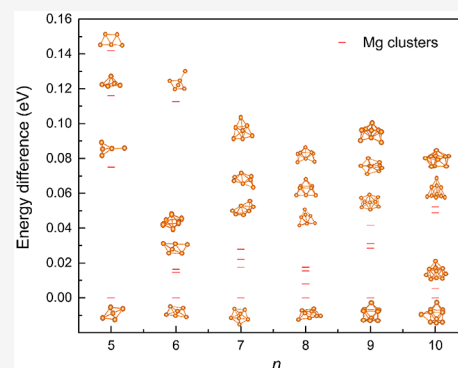
1. INTRODUCTION

In past decades, metal clusters have been intensively studied due to their importance in both basic research and potential technological applications in a range of areas such as heterogeneous catalysis,[1] nanoplasmonics,[2] chemical and biomolecular sensing,[3] and medicine.[4] The physicochemical properties of small metal clusters differ considerably from their corresponding atomic and bulk states and vary rapidly as the size of the cluster grows. The geometric structures of clusters determine their electronic structures, which further govern their physical and chemical properties. Therefore, identifying the geometric structures of metal clusters and underpinning the structure−property relationship are key issues in this research field since such knowledge is instrumental in designing metal clusters with tailored properties for practical applications. However, experimentally determining the real-space geometrical structures of small clusters is exceedingly difficult.[5,6] In practice, structural information on small clusters is most often obtained from theoretical studies or by a combination of theoretical simulations and experimental spectroscopic measurements.[7−15]

Theoretically, one can use first-principles quantum mechanical approaches to describe small atomic clusters. Kohn−Sham (KS) density functional theory (DFT)[16] within its conventional semilocal or hybrid functional approximations is the most widely used first-principles approach to describing the geometries and ground-state energies of clusters with up to ∼10^2 atoms. However, because of the exponentially increasing number of local minima in the potential energy surface, identifying the geometries of the energetically stable and low-lying metastable isomers is not at all trivial. In the past 30

years, several atomistic structure prediction algorithms have been developed, such as simulated annealing,[17] basin hopping,[18] genetic algorithms,[19−22] and the particle swarm optimization (PSO) algorithm,[23−25] allowing for efficiently locating the low-lying energy minima of a complex, high-dimensional potential energy surface. Indeed, when combined with density functional approximations (DFAs), these algorithms have enabled an efficient determination of the stable and metastable structures for molecules, clusters, and crystalline solids. In particular, the PSO-based CALYPSO (Crystal structure AnaLYsis by Particle Swarm Optimization) method, developed by Wang et al.,[24,25] has been widely used by the material science community and facilitated the discovery of a wide range of functional materials.[26]

Once the geometries of the clusters are determined, one can further study their detailed electronic structures, particularly the energy levels of the frontier orbitals, which in turn dictate their major physiochemical properties. In addition to the ground-state density and energy, Kohn−Sham DFT provides a set of auxiliary eigenorbitals and orbital energies, which are often used to describe one-electron excitation properties of the system. However, strictly speaking, only the energy levels of the highest occupied molecular orbital (HOMO) within
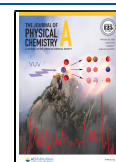
(generalized) KS theory[27] and the lowest unoccupied molecular orbital (LUMO) within generalized KS theory have physical meaning.[28] They correspond to the negative of the ionization potential (IP) and electron affinity (EA) of the system, respectively. In practice, the local and semilocal functionals often severely underestimate the IPs and overestimate the EAs, leading to fundamental energy gaps that are too small. Furthermore, the results from hybrid density functionals depend critically on the mixing and/or screening parameters. In this regard, the recently developed optically tuned range-separated hybrid functional seems to provide a good description of IPs and EAs for a wide range of molecules[29] and represents the current state of the art of generalized KS theory. An alternative yet more versatile and systematic approach to the electronic structure properties of materials is the many-body perturbation theory (MBPT) formulated in terms of the Green function.[30] The most widely used Green-function-based MBPT for describing real materials is the *GW* approximation of Hedin.[31] Indeed, the *GW* approximation has been the state-of-the-art approach for describing the band gaps of semiconductors during the last three decades[32−34] and is becoming increasingly popular for describing molecules and clusters.[35−40] Benchmark calculations indicate that *GW*-based methods can yield rather accurate IPs and EAs for small molecules[41] and capture long-range polarization effects in conjugated molecules.[42]

In this work, we employ a two-step approach to study the behavior of the IP and EA values of small alkali-earth metal clusters, specifically the beryllium and magnesium clusters (Be_n and Mg_n with $n \leq 20$). In the first step, we use the CALYPSO method/code, interfaced with the recently developed first-principles code package ABACUS,[43,44] to determine the geometries of the energetically low-lying isomers of the metal clusters. In the second step, the G_0W_0 method is used to calculate the IPs and EAs for the two sets of clusters. This is done using the FHI-aims code package.[36,45] The advantage of such a two-step approach is that the IPs and EAs, which are of vital importance to the physicochemical properties of the clusters, can be systematically and reliably calculated not only for the energetically most stable isomer but also for the low-lying metastable ones. In a typical experimental setup, the metastable structures are also accessible and influenced the overall properties of the cluster systems at finite temperatures. In this article, we report a study of Be and Mg clusters as a first application of this two-step approach. More investigations of clusters of other elements using this approach are ongoing.

Because of their closed outer s subshells, the atomic bonding character in alkali earth (group II) metal clusters gradually evolves from a dominating van der Waals (vdW) type to a metallic type, as the size of the cluster grows. This behavior renders the properties of small alkali earth metal clusters distinct from those of the more jellium-like alkali metal clusters as well as the more intriguing transition-metal and noble metal clusters. The Be bulk metal is an industrially important material, especially for aerospace applications, owing to its special properties such as high stability, light weight, and high melting temperature. However, there is so far little experimental information available for Be clusters, except for the Be dimer.[46] The studies on Be clusters are mainly theoretical,[47−52] and the multireference nature of the electronic structure of small Be clusters is of particular theoretical interest.[53,54] In contrast to Be clusters, there have been several experimental studies on Mg clusters.[55−58] On the

theoretical side, considerable effort has been devoted to investigating the transition from nonmetal to metal behavior[56,59,60] as the size of the clusters increases and the energetically global minimum geometries[61−63] as well as their electronic structure properties.[57,64] In these studies, the structural stability of consecutive clusters is analyzed in depth in terms of the binding energies and reactivity. The IP and EA properties are mostly obtained in terms of KS orbital energies and/or the Δ-SCF method[65−67] (i.e., the energy difference between the neutral and singly charged clusters). The *GW* method has been used to calculate the IPs of small Mg clusters[68] and the lifetime of the Mg_{40} cluster, but to the best of our knowledge, *GW* has not been used to compute the IPs and EAs of Be clusters. In this work, we will present systematic G_0W_0 benchmark calculations for all the low-lying isomers of Be_n and Mg_n clusters.

To make this research self-contained, we start by identifying the globally stable and low-lying metastable geometrical structures of Be_n and Mg_n clusters for $2 \leq n \leq 20$. The geometries are further optimized using the all-electron DFT method, and G_0W_0 calculations, based on preceding DFT calculations, are then performed for each of the clusters. The IP and EA values of these clusters are then obtained and compared to the results obtained by other studies. The reasons that we are looking at not only the most stable structure but also the metastable ones are the following. First, the abundance of the metastable isomers is proportional to Boltzmann factor $e^{-\Delta E/\kappa_B T}$, where ΔE is the energy difference in the metastable isomers with respect to the most stable one. Thus, the metastable isomers with a small ΔE also have a large chance to be present under the experimental conditions. Second, because of the limitation of the accuracy of the current DFAs as well as the precision of numerical implementations, the energy hierarchy of different isomers of a given cluster size may not be completely reliable. Thus, the computationally determined low-lying metastable structure may turn out to be the most stable one in reality.

2. COMPUTATIONAL METHODOLOGY

The geometrical structures of the stable and metastable isomers of Be_n and Mg_n clusters are searched using the CALYPSO code,[24,25] interfaced with the first-principles calculator—the ABACUS code[43,44]—with which the DFT calculations and local geometry relaxations are carried out. The generalized gradient approximation (GGA) of Perdew, Burke, and Ernzerhof (PBE)[69] for the exchange-correlation functional is employed in Kohn−Sham (KS) DFT calculations. Structure searching using the CALYPSO algorithm is terminated after 15 generations. The ABACUS code employs the ONCV-type multiprojector pseudopotentials, as provided by the SG15 library,[70] to describe the core ions. The energy cutoff for determining the uniform real-space integration grid and for solving the Poisson equations via fast Fourier transform is set to be 100 Ry. The triple-ζ plus double polarization (TZDP) numerical atomic orbitals (NAOs) are used to expand the KS wave functions. To determine how the results are converged with respect to the basis set size, we performed basis set convergence studies for Be_5 and Mg_5 clusters, and the results are presented in Figure S7 in the Supporting Information (SI). The tests indicate that TZDP or even the double-ζ plus polarization (DZP) basis set is adequate to obtain reliable cohesive energies and energy differences between different isomers. To describe the van der Waals (vdW) interactions

which might be important for small metal clusters, one simple approach is to complement PBE with the Grimme dispersion correction (PBE-D3).[71] In this work, PBE-D3 calculations are also performed for low-energy isomers, and the obtained results will be compared to the PBE results.

The initial geometries of the stable and metastable isomers of Be_n and Mg_n clusters are further relaxed using the all-electron FHI-aims code[45] with the same PBE functional in order to eliminate possible errors from the pseudopotential approximation. The G_0W_0 calculations based on the PBE reference state (denoted as G_0W_0@PBE) are then performed using the FHI-aims code.[36,45] For the geometry relaxation, the "tight" numerical setting and basis set are employed, whereas the larger NAO tier 3 (for Be_n) and tier 4 (for Mg_n) basis sets are used for G_0W_0@PBE calculations. In our G_0W_0 implementation, all of the molecular states generated from a given NAO basis set are included in the G_0W_0 calculations, following the so-called sum-overstates approach. Within such a formalism, the convergence is purely controlled by the size of the NAO basis set. Our previous experience indicates that the basis sets employed in the present work typically yield an accuracy better than 0.1 eV for IPs and EAs with respect to the complete basis set limit.

To double check the reliability of the energy hierarchy determined by ABACUS for Be_{14}, Mg_{14}, and Mg_{16} clusters, the low-lying isomers of these clusters are further calculated by both FHI-aims and Vienna ab initio simulation package (VASP)[72−74] codes. The plane-wave energy cutoff in the case of VASP was selected to be 450 eV for Be and 350 eV for Mg.

3. RESULTS AND DISCUSSION

In this section, we will first present the geometrical structures of stable and metastable Be_n and Mg_n clusters as determined by the CALYPSO method at the PBE level. In particular, we will discuss the newly found most stable isomer structures (at the PBE level) for Be_{14}, Mg_{14}, and Mg_{16} clusters. We then check the relative stability of low-energy isomers of these clusters using the PBE-D3 method. This is followed by a discussion of the binding energies (BEs) of the clusters. Finally, the IPs, EAs, and HOMO−LUMO gaps for the entire series of clusters as determined by G_0W_0@PBE are then presented and analyzed.

3.1. Geometrical Structures. *3.1.1. Novel Globally Stable Structures.* Among the Be_n and Mg_n ($2 \leq n \leq 20$) clusters studied in this work, we discuss in detail only the structures of the energetically low-lying isomers of Be_{14}, Mg_{14}, and Mg_{16} clusters. For these clusters, we have globally identified the most stable isomer structures, which to our knowledge have not been reported in the literature so far. For clusters of other sizes, the stable and low-lying metastable structures found in the present work are consistent with previous studies reported in the literature. These are included in the Supporting Information (Figures S1−S6) for completeness.

For Be_{14}, the newly found lowest-energy structure is presented in Figure 1a, along with the structures of three low-lying metastable isomers presented in Figure 1b−d. The numbers in parentheses indicate the energy difference in the metastable structures with respect to the most stable one, an isomer (a) whose energy is set to zero, as determined by the ABACUS code. As can be seen in Figure 1a, the newly determined lowest-energy isomer has a double-layer structure consisting of a hexagon with six Be atoms at the corners and one in the center. The two hexagons rotate with respect to
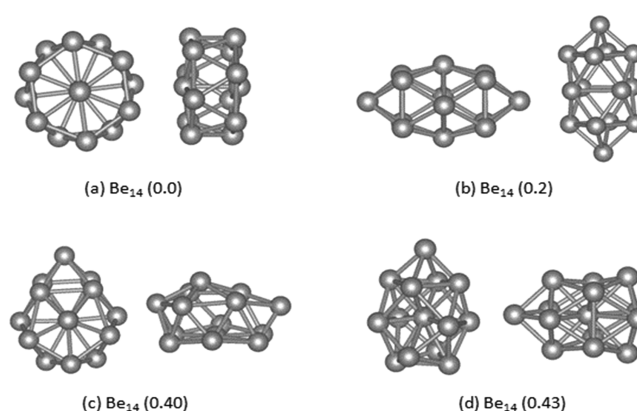

Figure 1. Geometrical structures of the most stable (a) and low-lying metastable (b−d) isomers of Be_{14} clusters. The numbers given in parentheses are the total energy difference (in eV) of the metastable isomers with respective to isomer (a) (whose energy is set to 0), as determined by ABACUS. For each isomer, structures viewed from two different perspectives are presented. The figures are plotted using the VESTA software tool.[75]

each other by 15°, thus the entire system has (approximate) S_6 symmetry. The isomer structure with the second-lowest energy can be viewed as a capped antiprism fused with a tetrahedral unit (cf. Figure 1b). The structures of Be_{14} isomers (c) and (d) are even higher in energy by 0.40 and 0.43 eV (as determined by ABACUS), respectively. Among all of these isomers, (b) and (d) were identified earlier by Sun and Fournier[52] and by Wang et al.,[47] respectively, as the lowest-energy structures for Be_{14}.

To determine if the ABACUS calculations have sufficient precision to pinpoint the lowest-energy structures, we also performed calculations using the FHI-aims and VASP codes to cross-validate the obtained results. In Table 1, the total energy

Table 1. Comparison of the Energetics of the Four Lowest-Energy Isomers of Be_{14} Isomers Obtained Using Three Codes: ABACUS, FHI-aims, and VASP[a]

	Energy difference with respect to the lowest-energy isomer (eV)				
	ABACUS (fully relaxed geometry)		FHI-aims (fully relaxed geometry)	FHI-aims (input geometry from ABACUS)	VASP (fully relaxed geometry)
Be_{14} isomers	DZP	TZDP			
(a)	0.0	0.0	0.0	0.0	0.0
(b)	0.195	0.044	0.006	0.005	0.033
(c)	0.409	0.381	0.581	0.690	0.593
(d)	0.433	0.435	0.391	0.392	0.408

[a]For FHI-aims calculations, both fully relaxed FHI-aims geometry and fixed-input ABACUS geometry are used. The energy of the isomer (a) obtained with each code is used as the respective energy reference (set to zero).

differences in isomers (b−d) with respect to isomer (a) of Be_{14} as obtained using ABACUS, FHI-aims, and VASP are presented. The ground-state total energy of isomer (a) obtained with each code is set to be the respective energy-zero reference. The FHI-aims calculations are made both with the fully relaxed geometry obtained by FHI-aims itself (third column of Table 1) and with fixed input geometry obtained by ABACUS (fourth column of Table 1).

The results presented in Table 1 indicate that all three codes consistently predict that isomer (a) is the energetically most stable structure among Be_{14} clusters. However, it appears that the energy difference between isomers (a) and (b) is overestimated by the ABACUS DZP results, and this overestimation can be corrected by going to the larger TZDP basis set. Furthermore, the energy ordering of isomers (c) and (d) is reversed in ABACUS, in contrast with FHI-aims and VASP. The FHI-aims calculations are made using both its own relaxed geometries and the input geometries as determined by ABACUS, and the results essentially stay the same. Because our major concern here is to separate the lowest-energy isomer from the metastable ones, we consider that ABACUS provides adequate accuracy for this purpose.

Also, we note that the validity of our finding that isomer (a) is energetically the most stable among Be_{14} clusters still depends on the accuracy of the PBE functional. There is a chance that PBE is not accurate in identifying the energetically most stable structure. Considering that the vdW interactions might be important for small alkali metal clusters, we also performed PBE-D3 calculations on these clusters. After further structural optimization using PBE-D3, the energy ordering remains the same for Be_{14} isomers. Under the circumstances in which clear experimental evidence is lacking, we tend to trust that the energy ordering provided by PBE/PBE-D3 is reliable. Nevertheless, we are currently investigating this issue with an accurate correlated method, which will allow us to draw more reliable conclusions regarding the energy ranking of the different isomers.

Next, we examine the geometries of the low-lying isomers of Mg_n clusters up to n = 20. In this case, we have identified new lowest-energy structures for Mg_{14} and Mg_{16} clusters, which will be discussed in detail below. For Mg_n clusters of other sizes, the structures of the lowest-energy isomers obtained in this work are consistent with what has been reported in the literature.[59,64,76,77] The structures of these clusters are presented in the Supporting Information (Figure S4) only for completeness. The structures of the low-lying metastable isomers are provided there (Figures S5 and S6).

The structures of the four lowest-energy isomers of Mg_{14} clusters as determined by CALYPSO in combination with ABACUS are presented in Figure 2. In contrast to the case of Be_{14} clusters, all four Mg_{14} isomers have low C_1 symmetry. Isomer (a), which is predicted to be the energetically most stable in the present work, has not been reported in the literature to the best of our knowledge. Isomers (b–d) are higher in energy by 0.05, 0.09, and 0.12 eV than isomer (a). Among these, isomers (b) and (c) in Figure 2 are consistent with the lowest-energy structures reported by Shen et al.[78] and by Duanmu et al.,[64] respectively.

To cross-check the validity of the above results obtained using ABACUS, we also performed FHI-aims and VASP calculations, and the obtained results are presented in Table 2 for comparison. In agreement with ABACUS, FHI-aims and VASP also predict that isomer (a) is energetically lowest whereas isomer (d) is energetically highest among the four isomers. However, the energy ordering of isomers (b) and (c) is changed within FHI-aims and VASP calculations, with isomer (c) remaining lower in energy than (b).

Finally, we examine the Mg_{16} clusters. The geometrical structures of the four lowest-energy isomers of Mg_{16} clusters are shown in Figure 3, and the ground-state energies as obtained by the three codes are presented in Table 2. All three
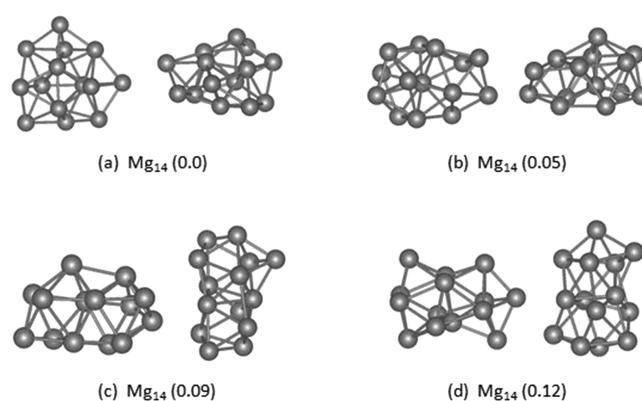

Figure 2. Geometrical structures of the most stable (a) and low-lying metastable (b–d) isomers of Mg_{14} clusters. The numbers given in parentheses are the total-energy difference (in eV) of the metastable isomers with respective to isomer (a) (whose energy is set to 0), as determined by ABACUS. For each isomer, structures viewed from two different perspectives are presented. The figures are plotted using the VESTA software tool.[75]

Table 2. Comparison of the Energetics of the Four Lowest-Energy Isomers of Mg_{14} and Mg_{16} Isomers Obtained Using Three Codes: ABACUS, FHI-aims, and VASP[a]

Mg_n isomers		Energy difference with respect to the lowest-energy isomer (eV)			
		ABACUS (fully relaxed geometry)	FHI-aims (fully relaxed geometry)	FHI-aims (input geometry from ABACUS)	VASP (fully relaxed geometry)
Mg_{14}	(a)	0	0	0	0
	(b)	0.052	0.039	0.046	0.040
	(c)	0.097	0.029	0.044	0.028
	(d)	0.127	0.100	0.132	0.103
Mg_{16}	(a)	0	0	0	0
	(b)	0.051	0.041	0.041	0.043
	(c)	0.102	0.131	0.208	0.131
	(d)	0.114	0.139	0.170	0.140

[a]For FHI-aims calculations, both fully relaxed FHI-aims geometry and fixed input ABACUS geometry are used. The energy of the isomer (a) obtained with each code is used as the respective energy reference (set to zero).

codes consistently predict that isomer (a), whose structure has not been reported in the literature before, is energetically the most stable, with an energy that is lower by 0.04–0.05 eV than that of isomer (b), which has C_{3v} symmetry and is next in the energy hierarchy. Furthermore, with their own fully relaxed structures, all three codes consistently yield the same energy ranking of the four isomers. Only those with fixed input geometry from ABACUS, the energies of isomers (c) and (d) as obtained by FHI-aims, are reordered. Among the four isomers of Mg_{16} determined in the present work, isomers (c) and (d) were reported by Shen et al.[78] and Jellinek et al.,[79] respectively, as the lowest-energy structures.

Similar to the Be_n cluster case, we also performed PBE-D3 calculations for Mg_n clusters. It turned out that the vdW corrections have more drastic effects on the Mg clusters. For Mg_{14} clusters, after further geometry relaxations with PBE-D3, the shapes of the structures of the energies of (a) and (b) isomers become very similar, with a tiny difference below 1 meV. For Mg_{16} clusters, isomers (c) and (d) are relaxed into the structures in which the dispersion contributions are added.
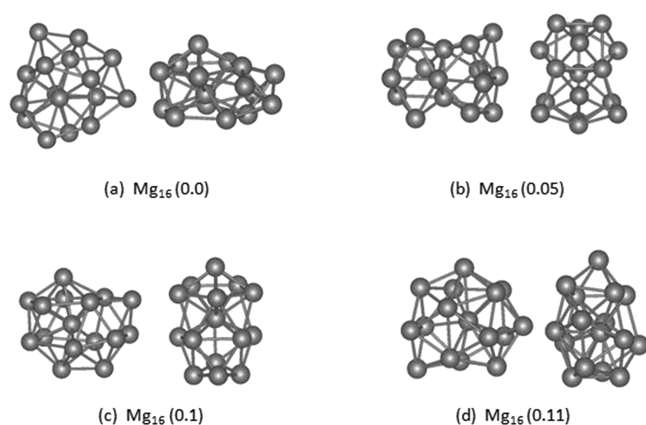
Figure 3. Geometrical structures of the most stable (*a*) and low-lying metastable (*b*–*d*) isomers of Mg_{16} clusters. The numbers given in the parentheses are the total-energy difference (in eV) of the metastable isomers with respective to isomer (*a*) (whose energy is set to 0), as determined by ABACUS. For each isomer, structures viewed from two different perspectives are presented. The figures are plotted using the VESTA software tool.[75]

In the meantime, their energies become very close to that of isomer (*a*), which retains its original PBE structure. Similar phenomena (i.e., originally distinct isomers collapsing into the same structure or the reordering of the energies of different isomers) also occur for Mg_5, Mg_{12}, and Mg_{19} clusters upon including the vdW corrections.

3.1.2. Structural Stability. An important indicator of the structural stability of metal clusters is the binding energy per atom, given by $E_b/n = (E_n - nE_{at})/n$ with E_n and E_{at} being the total energy of a cluster with n atoms and that of a single atom, respectively. Closely related to E_b/n is the second difference, defined as $\nabla_2 E_n = E_{n+1} + E_{n-1} - 2E_n$, signifying the relative stability of a cluster of size n with respect to its neighboring clusters. In this section, we will examine both the binding

energies and the second differences in Be_n and Mg_n clusters as a function of cluster size n.

The binding energies per atom for the lowest-energy isomers of Be_n clusters are shown in Figure. 4. Presented are the PBE and PBE-D3 results, as obtained in this work, as well as those obtained using other functionals, as reported in the literature. A feature common to all of the functionals is that the evolution of binding energies as a function of n exhibits three-stage behavior. From $n = 2$ to 4, there is a rapid increase in the binding energy, whereby the bonding characteristic develops from vdW type to metallic type. This is followed by the second stage from $n = 5$ to 10, where the increasing speed of the binding energy is slowed. From $n = 11$ on, the increase in the binding energy continues, but the increasing rate is further reduced. Despite this common overall feature, the magnitude of the binding energies obtained using different functionals differs significantly. Among these functionals, the L(S)DA functional gives the strongest binding, whereas the hybrid B3LYP functional gives the weakest binding, as expected. The binging strength of the PBE functional sits roughly in the middle. Adding vdW corrections, the PBE-D3 curve closely follows the PBE curve, with the binding strength only slightly increased. Further complications in Figure 4 come from the fact that the geometrical structures for some clusters determined in earlier works are not the most stable ones. The second differences, $\nabla_2 E_n$, in the Be_n clusters are presented in Figure 5, which clearly illustrates the relative stability of clusters of different sizes. Here, the pronounced peaks represent high stability, typically corresponding to a high abundance of the cluster size in experimental production. As can be seen from Figure 5, Be_n clusters with $n = 4$, 10, and 17 are very stable in the series, consistent with previous studies.[47] The Be_{14} cluster, with its newly identified lowest-energy structure, is also more stable (with a positive second difference) than its neighboring clusters (i.e., Be_{13} and Be_{15}). In ref 47, the Be_{13} and Be_{19} clusters are identified as "magic
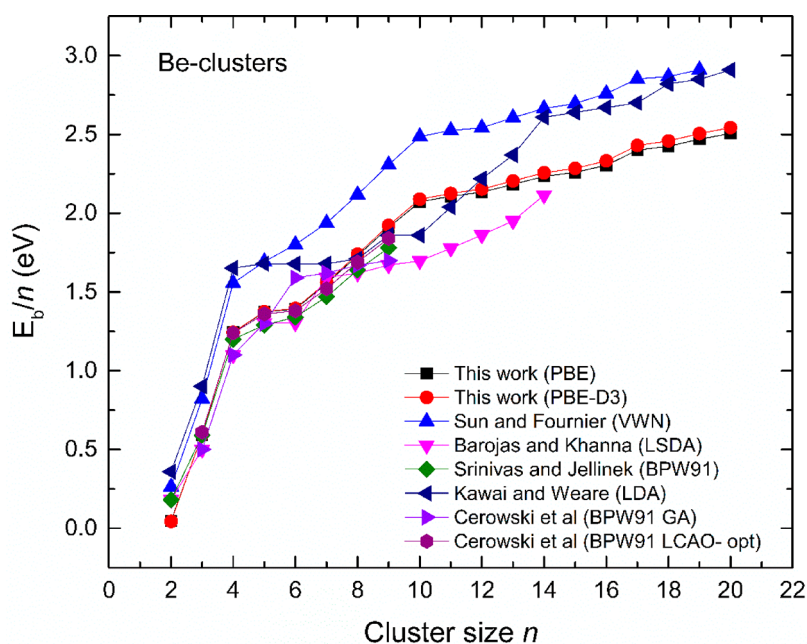

Figure 4. Binding energies per atom of neutral Be_n clusters as a function of cluster size n. The presented results are obtained using PBE (this work) and various other functionals such as VWN (the Vosko–Wilk–Nusair LSD functional),[52] LSDA,[81] LDA,[51] BPW91,[49,82] and B3LYP,[83] as reported in the literature.
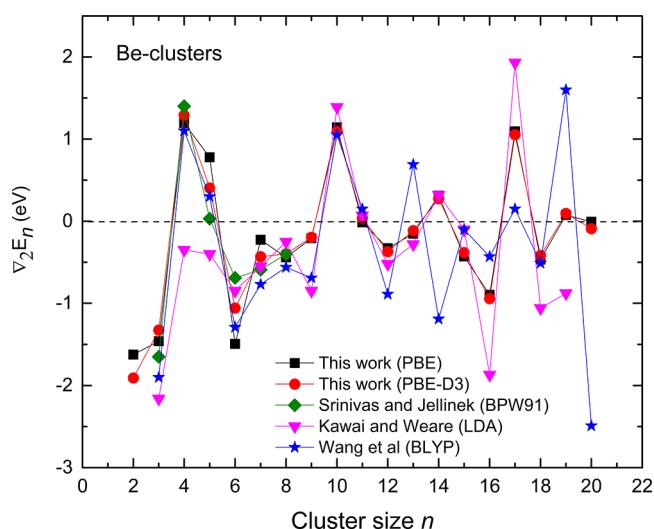
Figure 5. Second differences in the total energy $\nabla_2 E_n$ of Be_n clusters. The PBE results as obtained in this work are compared to those of other functionals—BPW91,[49] LDA,[51] and BLYP[47] as reported in the literature.

Figure 7. Second differences $\nabla_2 E_n$ of the total energy for Mg_n clusters as obtained in this work using the PBE functional, compared to the literature results obtained using various functionals: PW91,[86] B3PW91,[77] BP86,[80] and PBE.[59]

clusters" due to their exceptional stabilities. However, this is not the case in the present work or in refs 49 and 51. This difference might come from the different energy functionals used and possibly the different lowest-energy structures determined. This situation calls for more accurate functionals and more systematic structure prediction tools. The sizes of Be_n clusters with high stability are different from those of alkali metal clusters, with the latter being in better agreement with the prediction of the shell model.[60,80]

The binding energies and second differences in Mg_n clusters of size $2 \leq n \leq 20$ are presented in Figures 6 and 7, respectively. The overall trend in the binding energies of Mg_n clusters as a function of cluster size n is similar to that of the Be_n clusters, also exhibiting three-stage behavior. The magnitude of the binding energies of Mg_n clusters is much smaller than that of Be_n clusters, indicating that the Mg atoms bind together much more weakly than do the Be atoms. The
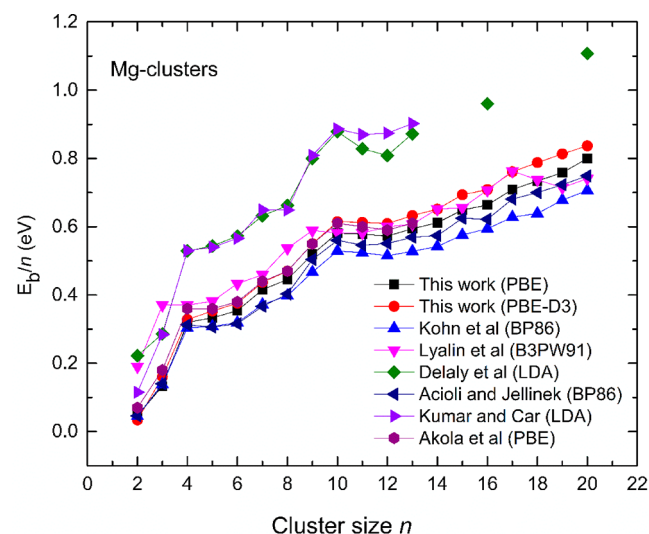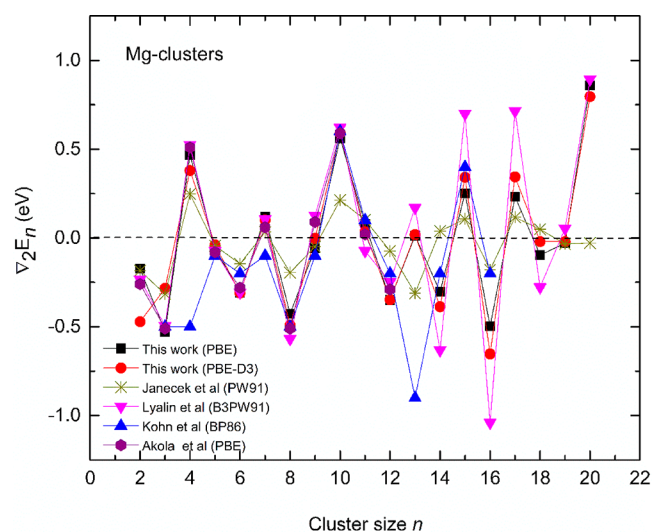

Figure 6. Binding energy per atom of neutral Mg clusters as a function of size, with a graphical comparison of this work (PBE) versus BP86,[61,80] B3PW91,[77] PBE,[59] and LDA.[60,84]

binding energy results obtained using various functionals show significant scattering, as shown in Figure 6. Among these, the PBE results obtained in this work are in good agreement with those of Akola et al.,[59] which are available only up to $n = 13$. Again, compared to various functionals, the PBE functional yields a binding strength that lies in the middle. Remarkably, the PBE results obtained in this work and those of Akola et al.[59] closely follow the B3PW91 results as obtained by Lyalin et al.[77] In their work, it was concluded that B3PW91 is more reliable than the commonly used B3LYP functional for studying the binding energy of Mg_n clusters. Adding dispersion corrections to PBE, the PBE-D3 binding energy curve shifts noticeably upward, exhibiting a gradually increasing vdW contribution to the binding energy that reaches approximately 0.05 eV/atom for $n \approx 20$. (See also Figure S8 in the Supporting Information.) Although the absolute magnitude of the vdW contributions in Mg clusters is similar to that in Be clusters (cf. Figure S8), their influence on the energy ordering of the different isomers appears to be stronger for Mg clusters. This is probably because the binding energies of Mg clusters at the GGA level are much weaker than those of Be clusters of the same size, and hence the vdW correction has a much larger proportion in the binding energies of Mg clusters. That is to say, the vdW contributions are more important to the Mg clusters on the relative scale.

The second differences $\nabla_2 E_n$ in the total energy for Mg_n clusters as presented in Figure 7 signify the cluster sizes with high stability. In this case, with rare exceptions, the results yielded by different functionals, as reported in different studies, show a qualitatively similar trend. Again, the PBE results as obtained in this work agree with the PBE results of Akola et al.[59] and the B3PW91 results of Lyalin et al.[77] to high precision. Adding dispersion corrections to PBE does not change the relative stability of consecutive clusters. In addition to the usual magic cluster sizes of $n = 4$, 10, and 20 as predicted by the shell model, clusters with $n = 7$, 15, and 17 also have a rather high stability. The stability of these clusters can be interpreted by the ellipsoidal shell distortions which typically occur in metallic clusters rather than by the spherical shell model.[85] The Mg_{14} and Mg_{16} clusters, where new lowest-
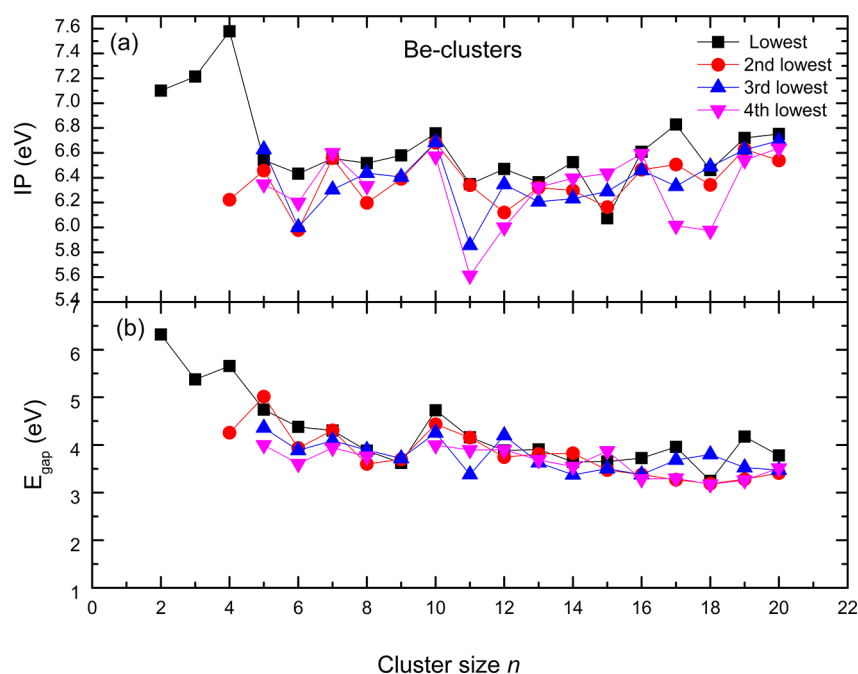
Figure 8. Vertical IPs (a) and HOMO−LUMO gaps (b) of Be_n clusters as a function of the cluster size. Results are presented, if available, for clusters up to the fourth-lowest-energy isomers.

energy structures are found, are not as stable as their neighboring clusters (i.e., Mg_{13}, Mg_{15}, and Mg_{17} clusters).

3.2. Electronic Properties. In this section, we present the IPs and HOMO−LUMO gaps of the Be_n and Mg_n clusters obtained by the G_0W_0 approach on the basis of the PBE starting point. The G_0W_0@PBE calculations are made using the FHI-aims code,[36,45] for which the input geometries of the Be_n and Mg_n clusters obtained from ABACUS are further relaxed. We also performed G_0W_0@PBE based on the PBE-D3 geometries as determined by ABACUS, but the obtained results do not show appreciable differences, particularly for the global minima structures. For simplicity, here we present only the G_0W_0 results based on the PBE geometries as determined by FHI-aims. We note that the IPs as given by G_0W_0 quasiparticle energy levels correspond to the so-called vertical ionization potentials (VIPs). The IP values presented in this paper are *de facto* the VIP ones.

3.2.1. Be_n Clusters. The G_0W_0@PBE IP values for Be_n clusters for $2 \leq n \leq 20$ are presented in the upper panel of Figure 8. Not only the results for the lowest-energy isomers but also those for the metastable ones are presented. For $n \geq 5$, results are provided up to the fourth lowest-energy isomers, except for $n = 9$, where only three distinct isomer structures are determined. For the lowest-energy isomers, the IP value first increases as n grows from 2 to 4, reaching its peak value of 7.6 eV at $n = 4$. From $n = 4$ to 5, the IP value quickly drops by more than 1 eV and then oscillates between 6.1 and 6.8 eV. Interestingly, the relatively more stable clusters (i.e., Be_4, Be_7, Be_{10}, and Be_{17} (cf. Figure 5)) also have a larger IP value compared to their neighbors, meaning that it costs more energy to ionize these clusters.

The IPs of the metastable Be_n clusters also oscillate as n grows, but their size evolution behavior is different from that of the lowest-energy isomers. For example, the IP of the metastable Be_4 cluster is smaller than its Be_5 counterpart (red dots in Figure 8), in contrast with the case of global minimum structures (black squares). Comparing the IPs of

most stable and metastable clusters, one noteworthy feature, as can be seen from Figure 8, is that the most stable isomer of a given cluster size usually has the largest IP. For cluster sizes of $n \leq 20$, $n = 5$, 7, and 15 represent exceptions.

In the literature,[49,52,82] the IPs of small Be_n clusters are mostly obtained using DFAs. In Figure S9 of the Supporting Information, we present a comparison of the G_0W_0@PBE IPs with those determined from DFAs. Our G_0W_0@PBE results are in good agreement with the Δ-SCF results of Srinivas and Jellineck[49] using the BPW91 GGA functional. However, the IP values directly obtained from the KS eigenvalues, as reported in refs 52 and 82, are significantly underestimated.

In Figure 8b, the HOMO−LUMO gaps (E_{gap}) of Be_n clusters as a function of n are presented. For the lowest-energy isomers, the gap value first systematically decreases from $n = 4$ to 9 and then increases by more than 1 eV from $n = 9$ to 10, signifying the extraordinary stability of the $n = 10$ cluster electronically. From $n = 10$ on, the energy gap decreases again until $n = 17$, the next cluster of high stability. The metastable clusters display behavior that closely follows that of the most stable clusters: the energy gap shows an overall piecewise decreasing behavior from $n = 4$ to 9 and from $n = 10$ to 18, with a sudden increase from $n = 9$ to 10. The energy gaps of the stable and low-lying metastable isomers can differ by as much as 1 eV. Furthermore, the energetically most stable isomers do not necessarily have the largest energy gap. For about half of the clusters with $n = 5−20$, the metastable isomers have a larger gap than the most stable isomer.

With the G_0W_0 IPs and HOMO−LUMO gaps presented, the G_0W_0 EAs are fully determined. For completeness, the G_0W_0@PBE EA values of Be_n clusters are presented in Table S1. As expected, the EA value increases as the cluster size grows, indicating an increasing capability to host an extra electron.

3.2.2. Mg_n Clusters. The IP values and HOMO−LUMO gaps of Mg_n clusters as a function of the size n are presented in Figure 9. Despite the presence of local oscillations, both the
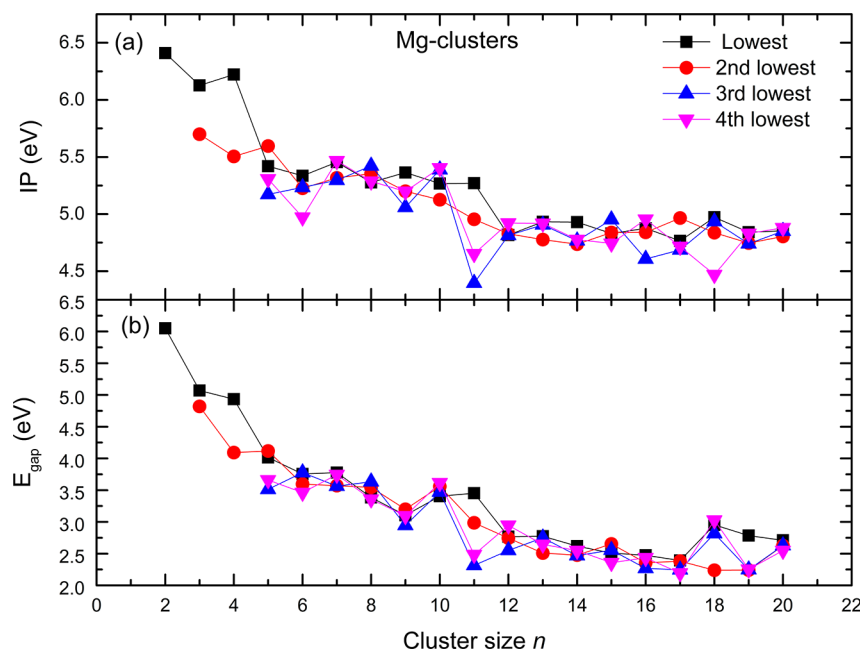
Figure 9. Vertical IPs (a) and HOMO−LUMO gaps (b) of Mg$_n$ clusters as a function of the cluster size. The results are presented, if available, for clusters up to the fourth-lowest-energy isomers.
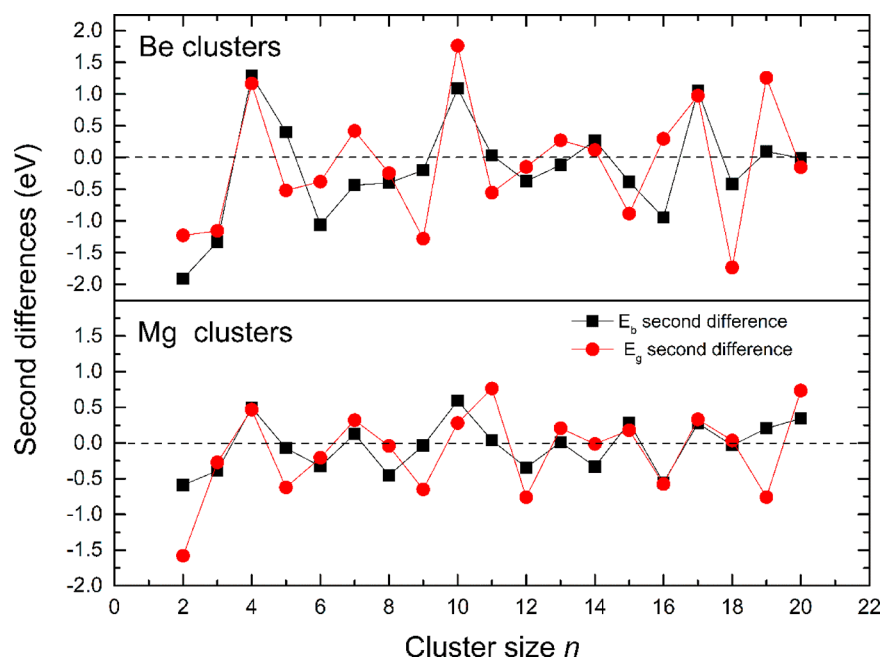

Figure 10. Second differences in the HOMO−LUMO gaps and binding energies for Be [upper panel] and Mg [lower panel] clusters as a function of cluster size n.

IPs and energy gaps show overall decreasing behavior as the cluster size grows. The behavior of the metastable clusters follows closely that of the lowest-energy ones. However, now neither the IPs nor the HOMO−LUMO gaps of the lowest-energy isomers show a characteristic feature which distinguishes them from the metastable ones. In particular, in contrast to the Be-cluster case where a predominant number of lowest-energy clusters have the largest IP, only 5 out of 18 different sizes of Mg$_n$ (n = 3−20) clusters show this behavior. In other words, neither the IPs nor the energy gaps of Mg$_n$ clusters can be used as a fingerprint to separate the globally most stable isomers from the metastable ones.

Considering all of the stable and metastable isomers, from the Mg dimer to Mg$_{20}$ clusters, the IP decreases from 6.5 eV to around 4.6 eV, which is still larger by about 1.0 eV than the work function of the Mg bulk metal (3.68 eV). The HOMO−LUMO gap decreases from 6 eV to approximately 2.5 eV, which is still sizable given that the bulk metal has a zero energy gap. This means that a 20-atom Mg cluster is still far from the bulk limit.

The EAs of Mg$_n$ clusters are presented in Table S2 of the Supporting Information. In contrast with the IPs, the EAs increase as the cluster size grows. A comparison of the G_0W_0@PBE IP values of the lowest-energy structures as computed in

this work with the results reported in the literature is presented in Figure S10. In addition to the DFA-based Δ-SCF results, another set of G_0W_0 (based on the LDA starting point) results as obtained by Zeng and He[68] are presented. Although the overall trends in the two sets of G_0W_0 results are the same, the IP values of Zeng and He are generally larger than ours. This difference is probably due to the details of the implementation and the different basis sets employed.

In addition to the IPs and HOMO−LUMO gaps, we also computed the G_0W_0@PBE density of states (DOS) for valence and low-lying conduction states. In Figure S11 of the Supporting Information, we presented the G_0W_0@PBE DOS for selected cluster sizes with $n = 4, 10, 14,$ and 20 atoms.

3.2.3. Correlation between the Structural Stability and the HOMO−LUMO Gap. One interesting question in cluster chemistry is if there is an underlying correlation between the relative thermodynamic stability of the clusters and their HOMO−LUMO gaps. To investigate this issue, we take the second difference of the binding energies as introduced in section 3.1.2 as a rough measure of the relative thermodynamic stability of consecutive clusters. Here, a large positive value of the second difference signifies the high stability of a given cluster compared to its neighbors. Similarly, one can also introduce a second difference of the HOMO−LUMO gap, given by $\nabla_2 E_g(n) = -[E_g(n + 1) + E_g(n - 1) - 2E_g(n)]$, whereby a positive second-difference value indicates a larger HOMO−LUMO gap of a given cluster of size n compared to its neighboring $(n - 1$ and $n + 1)$ clusters. The HOMO−LUMO gap of a cluster or a molecule can be interpreted as its chemical hardness.[87] According to the principle of maximum hardness (PMH), the molecules tend to arrange themselves so as to be as hard as possible under a given thermodynamic condition.[87−89] In the present context, this implies that the clusters with a larger HOMO−LUMO gap should have a higher abundance (i.e., should be chemically more stable). To check to what extent the PMH holds for Be_n and Mg_n clusters, we plot in Figure 10 the second differences in both the binding energies and the HOMO−LUMO as a function of the cluster size, n. One can see that, for both Be_n and Mg_n clusters, the peak structures and oscillation patterns of the second difference of the HOMO−LUMO gaps closely follow that of the binding energies, indicating a clear correlation between the structural stability and the chemical hardness of the metal clusters. To provide a quantitative estimate of how strong the correlation between the sets of quantities is, we plot in Figure S12 the second differences in the HOMO−LUMO gaps versus the second differences in the binding energies. The linear regression of the data returns a R^2 value of 0.41 for Be clusters and 0.39 for Mg clusters. The R^2 values are not very high, but a positive correlation between the types of second differences clearly exists.

4. CONCLUSIONS

We presented a systematic study of the structural and electronic properties of small Be and Mg clusters using a two-step approach. The structures of the Be_n and Mg_n clusters with $n = 2−20$ are determined using the CALYPSO structure prediction method based on the PBE potential energy surface, as computed using the ABACUS code. The electronic properties, specifically the IPs, the EAs, and the HOMO−LUMO gaps of the clusters, are obtained using the G_0W_0@PBE approach, as implemented in FHI-aims. Not only the globally lowest-energy isomer but also the low-lying (up to the fourth) metastable isomers are investigated.

At the DFT-PBE level, we identified novel globally lowest-energy structures for Be_{14}, Mg_{14}, and Mg_{16} clusters, which have not been reported in the literature to the best of our knowledge. This finding has been confirmed by a cross-check using three different first-principles codes. We also investigated the possible influence of the vdW interactions using the PBE-D3 method. While the dispersion corrections have little influence on the energy ordering of the Be clusters, much stronger impacts on the Mg clusters are observed. In the latter case, more accurate correlation methods that account for metallic and vdW bondings on the same footing should be applied to reach more reliable conclusions.

Furthermore, the G_0W_0@PBE IP and HOMO−LUMO gap results revealed the characteristic size evolution behavior of the alkali metal clusters. For Be_n clusters, although the low-energy isomers tend to have the largest IP value for each cluster size, exceptions do exist. For Mg_n clusters, this rule does not hold any longer. In general, it is not possible to distinguish the energetically most stable isomer from the metastable one just from the IPs or HOMO−LUMO gaps. On the other hand, the second-difference analysis of the consecutive clusters for both the binding energies and HOMO−LUMO gaps reveals a clear correlation of the structural stability and the chemical hardness of the lowest-energy isomers.

Finally, we remark that the combination of ground-state DFT, the unbiased structural search algorithm, and the Green-function-based quasiparticle method leads to a powerful approach to systematically investigating the structural and electronic properties of clusters. Applications of this combined two-step approach to other types of elemental clusters are underway.

■ ASSOCIATED CONTENT

ⓢ Supporting Information

The Supporting Information is available free of charge at https://pubs.acs.org/doi/10.1021/acs.jpca.0c08960.

> Structural properties, energetic properties, electronic structure properties, and geometry (XYZ) files for the clusters. (PDF)

■ AUTHOR INFORMATION

Corresponding Author

Xinguo Ren − *Beijing National Laboratory for Condensed Matter Physics, Institute of Physics, Chinese Academy of Sciences, Beijing 100190, China;* ⓞ orcid.org/0000-0002-3360-2281; Email: renxg@iphy.ac.cn

Authors

Sunila Bakhsh − *CAS Key Laboratory of Quantum Information, University of Science and Technology of China, Hefei, Anhui 230026, China; Balochistan University of Information Technology, Engineering and Management Sciences, Quetta, Pakistan*

Xiaohui Liu − *Supercomputing Center, University of Science and Technology of China, Hefei, Anhui 230026, China*

Yanyong Wang − *CAS Key Laboratory of Quantum Information, University of Science and Technology of China, Hefei, Anhui 230026, China*

Lixin He − *CAS Key Laboratory of Quantum Information, University of Science and Technology of China, Hefei, Anhui 230026, China*

Complete contact information is available at:
https://pubs.acs.org/10.1021/acs.jpca.0c08960

Notes

The authors declare no competing financial interest.

■ ACKNOWLEDGMENTS

■ REFERENCES

(1) Liu, L.; Corma, A. Metal Catalysts for Heterogeneous Catalysis: From Single Atoms to Nanoclusters and Nanoparticles. *Chem. Rev.* **2018**, *118* (10), 4981−5079.

(2) Schuller, J. A.; Barnard, E. S.; Cai, W.; Jun, Y. C.; White, J. S.; Brongersma, M. L. Plasmonics for Extreme Light Concentration and Manipulation. *Nat. Mater.* **2010**, *9* (3), 193−204.

(3) Mathew, A.; Pradeep, T. Noble Metal Clusters: Applications in Energy, Environment, and Biology. *Part. Part. Syst. Charact.* **2014**, *31* (10), 1017−1053.

(4) Leśnikowski, Z. J. Challenges and Opportunities for the Application of Boron Clusters in Drug Design. *J. Med. Chem.* **2016**, *59* (17), 7738−7758.

(5) Meng, G.; Arkus, N.; Brenner, M. P.; Manoharan, V. N. The Free-Energy Landscape of Clusters of Attractive Hard Spheres. *Science (Washington, DC, U. S.)* **2010**, *327* (5965), 560−563.

(6) Johnston, R. L. *Atomic and Molecular Clusters*; CRC Press, 2002, DOI: 10.1201/9780367805814.

(7) Bonacic-Koutecky, V.; Fantucci, P.; Koutecky, J. Quantum Chemistry of Small Clusters of Elements of Groups Ia, Ib, and IIa: Fundamental Concepts, Predictions, and Interpretation of Experiments. *Chem. Rev.* **1991**, *91* (5), 1035−1108.

(8) Furche, F.; Ahlrichs, R.; Weis, P.; Jacob, C.; Gilb, S.; Bierweiler, T.; Kappes, M. M. The Structures of Small Gold Cluster Anions as Determined by a Combination of Ion Mobility Measurements and Density Functional Calculations. *J. Chem. Phys.* **2002**, *117* (15), 6982−6990.

(9) Parks, E. K.; Zhu, L.; Ho, J.; Riley, S. J. The Structure of Small Nickel Clusters. I. Ni$_3$ − Ni$_{15}$. *J. Chem. Phys.* **1994**, *100* (10), 7206−7222.

(10) Jackschath, C.; Rabin, I.; Schulze, W. Electronic Structures and Related Properties. Electron Impact Ionization Potentials of Gold and Silver Clusters Men, *n* ≤ 22. *Berichte der Bunsengesellschaft für Phys. Chemie* **1992**, *96* (9), 1200−1204.

(11) Bravo-Pérez, G.; Garzón, I. L.; Novaro, O. Ab Initio Study of Small Gold Clusters. *J. Mol. Struct.: THEOCHEM* **1999**, *493* (1−3), 225−231.

(12) Nayak, S. K.; Khanna, S. N.; Rao, B. K.; Jena, P. Physics of Nickel Clusters: Energetics and Equilibrium Geometries. *J. Phys. Chem. A* **1997**, *101* (6), 1072−1080.

(13) Tai, T. B.; Grant, D. J.; Nguyen, M. T.; Dixon, D. A. Thermochemistry and Electronic Structure of Small Boron Clusters (B$_n$, n= 5−13) and Their Anions. *J. Phys. Chem. A* **2010**, *114* (2), 994−1007.

(14) Blanc, J.; Bonačić-Koutecký, V.; Broyer, M.; Chevaleyre, J.; Dugourd, P.; Koutecký, J.; Scheuch, C.; Wolf, J. P.; Wöste, L.

(15) Evolution of the Electronic Structure of Lithium Clusters between Four and Eight Atoms. *J. Chem. Phys.* **1992**, *96* (3), 1793−1809.

(15) Wang, L.-S. Photoelectron Spectroscopy of Size-Selected Boron Clusters: From Planar Structures to Borophenes and Borospherenes. *Int. Rev. Phys. Chem.* **2016**, *35* (1), 69−142.

(16) Kohn, W.; Sham, L. J. Self-Consistent Equations Including Exchange and Correlation Effects. *Phys. Rev.* **1965**, *140* (4A), A1133−A1138.

(17) Wille, L. T. Minimum-Energy Configurations of Atomic Clusters: New Results Obtained by Simulated Annealing. *Chem. Phys. Lett.* **1987**, *133* (5), 405−410.

(18) Wales, D. J.; Doye, J. P. K. Global Optimization by Basin-Hopping and the Lowest Energy Structures of Lennard-Jones Clusters Containing up to 110 Atoms. *J. Phys. Chem. A* **1997**, *101* (28), 5111−5116.

(19) Deaven, D. M.; Ho, K. M. Molecular Geometry Optimization with a Genetic Algorithm. *Phys. Rev. Lett.* **1995**, *75* (2), 288−291.

(20) Woodley, S. M.; Battle, P. D.; Gale, J. D.; Catlow, C. R. A. The Prediction of Inorganic Crystal Structures Using a Genetic Algorithm and Energy Minimisation. *Phys. Chem. Chem. Phys.* **1999**, *1* (10), 2535−2542.

(21) Glass, C. W.; Oganov, A. R.; Hansen, N. USPEX-Evolutionary Crystal Structure Prediction. *Comput. Phys. Commun.* **2006**, *175* (11−12), 713−720.

(22) Wu, S. Q.; Ji, M.; Wang, C. Z.; Nguyen, M. C.; Zhao, X.; Umemoto, K.; Wentzcovitch, R. M.; Ho, K. M. An Adaptive Genetic Algorithm for Crystal Structure Prediction. *J. Phys.: Condens. Matter* **2014**, *26* (3), 035402−14.

(23) Kennedy, J.; Eberhart, R. C. Discrete Binary Version of the Particle Swarm Algorithm. *Proc. IEEE Int. Conf. Syst. Man Cybern.* **1997**, *5*, 4104−4108.

(24) Wang, Y.; Lv, J.; Zhu, L.; Ma, Y. Crystal Structure Prediction via Particle-Swarm Optimization. *Phys. Rev. B: Condens. Matter Mater. Phys.* **2010**, *82* (9), 094116.

(25) Wang, Y.; Lv, J.; Zhu, L.; Ma, Y. CALYPSO: A Method for Crystal Structure Prediction. *Comput. Phys. Commun.* **2012**, *183* (10), 2063−2070.

(26) Wang, Y.; Ding, Y. Unexpected Buckled Structures and Tunable Electronic Properties in Arsenic Nanosheets: Insights from First-Principles Calculations. *J. Phys.: Condens. Matter* **2015**, *27* (22), 225304.

(27) Janak, J. F. Proof That $\partial E \partial n i = \varepsilon$ in Density-Functional Theory. *Phys. Rev. B: Condens. Matter Mater. Phys.* **1978**, *18* (12), 7165−7168.

(28) Yang, W.; Cohen, A. J.; Mori-Sánchez, P. Derivative Discontinuity, Bandgap and Lowest Unoccupied Molecular Orbital in Density Functional Theory. *J. Chem. Phys.* **2012**, *136* (20), 204111.

(29) Kronik, L.; Stein, T.; Refaely-Abramson, S.; Baer, R. Excitation Gaps of Finite-Sized Systems from Optimally Tuned Range-Separated Hybrid Functionals. *J. Chem. Theory Comput.* **2012**, *8* (5), 1515−1531.

(30) Fetter, A. L.; Walecka, J. D.; Kadanoff, L. P. Quantum Theory of Many Particle Systems. *Phys. Today* **1972**, *25* (11), 54−55.

(31) Hedin, L. New Method for Calculating the One-Particle Green's Function with Application to the Electron-Gas Problem. *Phys. Rev.* **1965**, *139* (3A), A796−A823.

(32) Hybertsen, M. S.; Louie, S. G. Electron Correlation in Semiconductors and Insulators: Band Gaps and Quasiparticle Energies. *Phys. Rev. B: Condens. Matter Mater. Phys.* **1986**, *34* (8), 5390−5413.

(33) Aryasetiawan, F.; Gunnarsson, O. The GW Method. *Rep. Prog. Phys.* **1998**, *61* (3), 237−312.

(34) Golze, D.; Dvorak, M.; Rinke, P. The GW Compendium: A Practical Guide to Theoretical Photoemission Spectroscopy. *Front. Chem.* **2019**, *7* (July), DOI: 10.3389/fchem.2019.00377.

(35) Noguchi, Y.; Ishii, S.; Ohno, K.; Sasaki, T. Quasiparticle Energy Spectra of Alkali-Metal Clusters: All-Electron First-Principles Calculations. *J. Chem. Phys.* **2008**, *129* (10), 104104.

(36) Ren, X.; Rinke, P.; Blum, V.; Wieferink, J.; Tkatchenko, A.; Sanfilippo, A.; Reuter, K.; Scheffler, M. Resolution-of-Identity

Approach to Hartree−Fock, Hybrid Density Functionals, RPA, MP2 and GW with Numeric Atom-Centered Orbital Basis Functions. *New J. Phys.* **2012**, *14* (5), 053020.

(37) Bruneval, F.; Marques, M. A. L. Benchmarking the Starting Points of the GW Approximation for Molecules. *J. Chem. Theory Comput.* **2013**, *9* (1), 324−329.

(38) van Setten, M. J.; Caruso, F.; Sharifzadeh, S.; Ren, X.; Scheffler, M.; Liu, F.; Lischner, J.; Lin, L.; Deslippe, J. R.; Louie, S. G.; Yang, C.; Weigend, F.; Neaton, J. B.; Evers, F.; Rinke, P. GW 100: Benchmarking G_0W_0 for Molecular Systems. *J. Chem. Theory Comput.* **2015**, *11* (12), 5665−5687.

(39) Ren, X.; Marom, N.; Caruso, F.; Scheffler, M.; Rinke, P. Beyond the GW Approximation: A Second-Order Screened Exchange Correction. *Phys. Rev. B: Condens. Matter Mater. Phys.* **2015**, *92* (8), 081104.

(40) Maggio, E.; Liu, P.; van Setten, M. J.; Kresse, G. GW 100: A Plane Wave Perspective for Small Molecules. *J. Chem. Theory Comput.* **2017**, *13* (2), 635−648.

(41) Knight, J. W.; Wang, X.; Gallandi, L.; Dolgounitcheva, O.; Ren, X.; Ortiz, J. V.; Rinke, P.; Körzdörfer, T.; Marom, N. Accurate Ionization Potentials and Electron Affinities of Acceptor Molecules III: A Benchmark of GW Methods. *J. Chem. Theory Comput.* **2016**, *12* (2), 615−626.

(42) Pinheiro, M.; Caldas, M. J.; Rinke, P.; Blum, V.; Scheffler, M. Length Dependence of Ionization Potentials of Transacetylenes: Internally Consistent DFT/GW Approach. *Phys. Rev. B: Condens. Matter Mater. Phys.* **2015**, *92* (19), 195134.

(43) Chen, M.; Guo, G.-C.; He, L. Systematically Improvable Optimized Atomic Basis Sets for Ab Initio Calculations. *J. Phys.: Condens. Matter* **2010**, *22* (44), 445501.

(44) Li, P.; Liu, X.; Chen, M.; Lin, P.; Ren, X.; Lin, L.; Yang, C.; He, L. Large-Scale Ab Initio Simulations Based on Systematically Improvable Atomic Basis. *Comput. Mater. Sci.* **2016**, *112*, 503−517.

(45) Blum, V.; Gehrke, R.; Hanke, F.; Havu, P.; Havu, V.; Ren, X.; Reuter, K.; Scheffler, M. Ab Initio Molecular Simulations with Numeric Atom-Centered Orbitals. *Comput. Phys. Commun.* **2009**, *180* (11), 2175−2196.

(46) Antonov, I. O.; Barker, B. J.; Bondybey, V. E.; Heaven, M. C. Spectroscopic Characterization of $Be_2^+ {}_X \sum_{2u}^+$ and the Ionization Energy of Be_2. *J. Chem. Phys.* **2010**, *133* (7), 074309.

(47) Wang, J.; Wang, G.; Zhao, J. Density Functional Study of Beryllium Clusters, with Gradient Correction. *J. Phys.: Condens. Matter* **2001**, *13* (33), L753−L758.

(48) Beyer, M. K.; Kaledin, L. A.; Kaledin, A. L.; Heaven, M. C.; Bondybey, V. E. Density Functional Calculations of Beryllium Clusters Be(n), n = 2−8. *Chem. Phys.* **2000**, *262* (1), 15−23.

(49) Srinivas, S.; Jellinek, J. Structural and Electronic Properties of Small Beryllium Clusters: A Theoretical Study. *J. Chem. Phys.* **2004**, *121* (15), 7243−7252.

(50) Lee, T. J.; Rendell, A. P.; Taylor, P. R. Comparison of the Quadratic Configuration Interaction and Coupled-Cluster Approaches to Electron Correlation Including the Effect of Triple Excitations. *J. Phys. Chem.* **1990**, *94*, 5463−5468.

(51) Kawai, R.; Weare, J. H. From van Der Waals to Metallic Bonding: The Growth of Be Clusters. *Phys. Rev. Lett.* **1990**, *65* (1), 80−83.

(52) Lee, T. J.; Rendell, A. P.; Taylor, P. R. Comparison of the Quadratic Configuration Interaction and Coupled-Cluster Approaches to Electron Correlation Including the Effect of Triple Excitations. *J. Phys. Chem.* **1990**, *94*, 5463−5468.

(53) Heaven, M. C.; Merritt, J. M.; Bondybey, V. E. Bonding in Beryllium Clusters. *Annu. Rev. Phys. Chem.* **2011**, *62* (1), 375−393.

(54) Sharma, S.; Yanai, T.; Booth, G. H.; Umrigar, C. J.; Chan, G. K.-L. Spectroscopic Accuracy Directly from Quantum Chemistry: Application to Ground and Excited States of Beryllium Dimer. *J. Chem. Phys.* **2014**, *140* (10), 104112.

(55) Balfour, W. J.; Douglas, A. E. Absorption Spectrum of the Mg 2 Molecule. *Can. J. Phys.* **1970**, *48* (7), 901−914.

(56) Thomas, O. C.; Zheng, W.; Xu, S.; Bowen, K. H. Onset of Metallic Behavior in Magnesium Clusters. *Phys. Rev. Lett.* **2002**, *89* (21), 213403.

(57) Kaufmann, A.; Kornath, A.; Zoermer, A.; Ludwig, R. Small Magnesium Clusters: Between van Der Waals and Valence Bonds. *Inorg. Chem.* **2010**, *49* (8), 3851−3856.

(58) Diederich, T.; Döppner, T.; Braune, J.; Tiggesbäumker, J.; Meiwes-Broer, K.-H. Electron Delocalization in Magnesium Clusters Grown in Supercold Helium Droplets. *Phys. Rev. Lett.* **2001**, *86* (21), 4807−4810.

(59) Akola, J.; Rytkönen, K.; Manninen, M. Metallic Evolution of Small Magnesium Clusters. *Eur. Phys. J. D* **2001**, *16* (1), 21−24.

(60) Delaly, P.; Ballone, P.; Buttet, J. Metallic Bonding in Magnesium Microclusters. *Phys. Rev. B: Condens. Matter Mater. Phys.* **1992**, *45* (7), 3838−3841.

(61) Acioli, P. H.; Jellinek, J. Electron Binding Energies of Anionic Magnesium Clusters and the Nonmetal-to-Metal Transition. *Phys. Rev. Lett.* **2002**, *89* (21), 213402.

(62) Zhao, J.; Chen, X.; Wang, G. Critical Size for a Metal-Nonmetal Transition in Transition-Metal Clusters. *Phys. Rev. B: Condens. Matter Mater. Phys.* **1994**, *50* (20), 15424−15426.

(63) Aguilera-Granja, F.; Bouarab, S.; Vega, A.; Alonso, J. A.; Montejano-Carrizales, J. M. Nonmetal-Metal Transition in Ni Clusters. *Solid State Commun.* **1997**, *104* (10), 635−639.

(64) Duanmu, K.; Friedrich, J.; Truhlar, D. G. Thermodynamics of Metal Nanoparticles: Energies and Enthalpies of Formation of Magnesium Clusters and Nanoparticles as Large as 1.3 Nm. *J. Phys. Chem. C* **2016**, *120* (45), 26110−26118.

(65) Tiago, M. L.; Idrobo, J. C.; Öğüt, S.; Jellinek, J.; Chelikowsky, J. R. Electronic and Optical Excitations in Ag n Clusters (N= 1–8): Comparison of Density-Functional and Many-Body Theories. *Phys. Rev. B: Condens. Matter Mater. Phys.* **2009**, *79* (15), 155419.

(66) Vydrov, O. A.; Scuseria, G. E. Ionization Potentials and Electron Affinities in the Perdew-Zunger Self-Interaction Corrected Density-Functional Theory. *J. Chem. Phys.* **2005**, *122* (18), 184107.

(67) Beste, A.; Harrison, R. J.; Yanai, T. Direct Computation of General Chemical Energy Differences: Application to Ionization Potentials, Excitation, and Bond Energies. *J. Chem. Phys.* **2006**, *125* (7), 074101.

(68) Zeng, T.; He, Y. Scaling of the Self-Energy Correction to the HOMO-LUMO Gap with Magnesium Cluster Size and Its Potential for Extrapolating to Larger Magnesium Clusters. *J. Appl. Phys.* **2018**, *124* (4), 044305.

(69) Perdew, J. P.; Burke, K.; Ernzerhof, M. Generalized Gradient Approximation Made Simple. *Phys. Rev. Lett.* **1996**, *77* (18), 3865−3868.

(70) Quantum simulation. http://www.quantum-simulation.org/potentials/sg15_oncv/, http://quantum-simulation.org/potentials/sg15_oncv/upf (accessed May 31, 2020).

(71) Grimme, S.; Antony, J.; Ehrlich, S.; Krieg, H. A Consistent and Accurate Ab Initio Parametrization of Density Functional Dispersion Correction (DFT-D) for the 94 Elements H-Pu. *J. Chem. Phys.* **2010**, *132* (15), 154104.

(72) Kresse, G.; Furthmüller, J. Efficient Iterative Schemes for Ab Initio Total-Energy Calculations Using a Plane-Wave Basis Set. *Phys. Rev. B: Condens. Matter Mater. Phys.* **1996**, *54* (16), 11169−11186.

(73) Kresse, G.; Furthmüller, J. Efficiency of Ab-Initio Total Energy Calculations for Metals and Semiconductors Using a Plane-Wave Basis Set. *Comput. Mater. Sci.* **1996**, *6* (1), 15−50.

(74) Kresse, G.; Joubert, D. From Ultrasoft Pseudopotentials to the Projector Augmented-Wave Method. *Phys. Rev. B: Condens. Matter Mater. Phys.* **1999**, *59* (3), 1758−1775.

(75) Momma, K.; Izumi, F. VESTA 3 for Three-Dimensional Visualization of Crystal, Volumetric and Morphology Data. *J. Appl. Crystallogr.* **2011**, *44* (6), 1272−1276.

(76) Zhang, J.-M.; Duan, Y.-N.; Xu, K.-W.; Ji, V.; Man, Z.-Y. Ab Initio Calculation of Neutral and Singly Charged Mg_n (n≤11) Clusters. *Phys. B* **2008**, *403* (18), 3119−3124.

(77) Lyalin, A.; Solov'yov, I. A.; Solov'yov, A. V.; Greiner, W. Evolution of the Electronic and Ionic Structure of Mg Clusters with Increase in Cluster Size. *Phys. Rev. A: At., Mol., Opt. Phys.* **2003**, *67* (6), 13.

(78) Shen, D.; Kong, C.-P.; Jia, R.; Fu, P.; Zhang, H.-X. Investigation of Properties of Mg n Clusters and Their Hydrogen Storage Mechanism: A Study Based on DFT and a Global Minimum Optimization Method. *J. Phys. Chem. A* **2015**, *119* (15), 3636−3643.

(79) Jellinek, J.; Acioli, P. H. Magnesium Clusters: Structural and Electronic Properties and the Size-Induced Nonmetal-to-Metal Transition. *J. Phys. Chem. A* **2002**, *106* (45), 10919−10925.

(80) Köhn, A.; Weigend, F.; Ahlrichs, R. Theoretical Study on Clusters of Magnesium. *Phys. Chem. Chem. Phys.* **2001**, *3* (5), 711−719.

(81) Blaisten-Barojas, E.; Khanna, S. N. Development of a First-Principles Many-Body Potential for Beryllium. *Phys. Rev. Lett.* **1988**, *61* (13), 1477−1480.

(82) Cerowski, V.; Rao, B. K.; Khanna, S. N.; Jena, P.; Ishii, S.; Ohno, K.; Kawazoe, Y. Evolution of the Electronic Structure of Be Clusters. *J. Chem. Phys.* **2005**, *123* (7), 074329.

(83) Ge, G.; Yan, Y.; Ren, F.; Lei, X.; Yang, Z.; Zhao, W.; Wang, Q. Density Functional Theory Study of Structure and Electronic Properties of $MgBe_n$ (n = 2-12) Clusters. *Chin. J. Chem. Phys.* **2007**, *20* (5), 518−524.

(84) Kumar, V.; Car, R. Structure, Growth, and Bonding Nature of Mg Clusters. *Phys. Rev. B: Condens. Matter Mater. Phys.* **1991**, *44* (15), 8243−8255.

(85) Clemenger, K. Ellipsoidal Shell Structure in Free-Electron Metal Clusters. *Phys. Rev. B: Condens. Matter Mater. Phys.* **1985**, *32* (2), 1359−1362.

(86) Janecek, S.; Krotscheck, E.; Liebrecht, M.; Wahl, R. Structure of Mg_n and Mg_n^+ up to n = 30. *Eur. Phys. J. D* **2011**, *63*, 377−390.

(87) Parr, R. G.; Chattaraj, P. K. Principle of Maximum Hardness. *J. Am. Chem. Soc.* **1991**, *113* (5), 1854−1855.

(88) Pearson, R. G. Recent Advances in the Concept of Hard and Soft Acids and Bases. *J. Chem. Educ.* **1987**, *64* (7), 561.

(89) Pearson, R. G. Hard and Soft Acids and Bases, Dowden, Hutchinson and Ross, Stroudsberg, PA, 1973 Search PubMed;(b) RG Pearson. *Acc. Chem. Res.* **1993**, *26*, 250−255.